Dielectric Relaxation Processes in Ethanol/Water Mixtures

Takaaki Sato*

Division of Pure and Applied Physics, Graduate School of Science and Engineering, Waseda University, Okubo, Shinjuku-ku, Tokyo 169-8555, Japan

Richard Buchner

Institut für Physikalische und Theoretische Chemie, Universität Regensburg, D-93040 Regensburg, Germany

Received: May 8, 2003; In Final Form: March 29, 2004

We have determined the complex dielectric spectra of ethanol/water mixtures at 25 °C for the nine molar fractions of ethanol, $X_{EA} = 0.04$, 0.08, 0.11, 0.18, 0.3, 0.5, 0.7, 0.9, and 1.0, in the frequency range $0.1 \leq \nu/\text{GHz} \leq 89$ using TDR in $0.1 \leq \nu/\text{GHz} \leq 25$ and waveguide interferometers in $13 \leq \nu/\text{GHz} \leq 89$. At $0.3 \leq X_{EA} \leq 1.0$, a three-step relaxation model turns out to be most appropriate. Besides a Cole−Cole relaxation for the dominating low-frequency process ($j = 1$), assigned to the cooperative dynamics of the H-bond system, which exhibits a pronounced increase of its relaxation time, τ_1, when going from $X_{EA} = 0$ to 1, two additional Debye terms ($j = 2$ and 3) with the relaxation times of $\tau_2 \approx 10$ ps and $\tau_3 \approx 1-2$ ps are required to reproduce the high-frequency part of the spectrum. In view of the well-established relaxation mechanisms of pure liquids, these high-frequency processes can be validly assigned to the motion of singly H-bonded ethanol monomers at the ends of the chain structure ($j = 2$) and the flipping motion of free OH ($j = 3$), respectively. The unusual increase of the amplitude $\Delta\epsilon_2$ with decreasing X_{EA} in $\sim 0.5 \leq X_{EA} \leq 1.0$ suggests insertion of water molecules into the zigzag structure of winding H-bonded ethanol chains resulting in a reduction of the average chain length and an increase of the number of end-standing ethanol molecules that can contribute to the τ_2-mode. At $X_{EA} < 0.3$, τ_1 rapidly approaches τ_2 and $\Delta\epsilon_2 \rightarrow 0$, so that the intermediate ethanol monomer process ($j = 2$) becomes inseparable while the fast switching process with $\tau_3 \approx 1$ ps can always be resolved. The analysis of the effective dipolar correlation factor, g_{eff}, revealed that the parallel arrangement of dipole vectors of ethanol molecules is fairly disturbed by the presence of a small amount of water. Water has a strong perturbation effect on the ethanol hydrogen-bonding chain structure in the ethanol-rich region of $0.3 \leq X_{EA} \leq 1.0$.

1. Introduction

Due to the amphiphilic nature of monohydric alcohols, they interact with water through hydrogen bonding and at the same time seem to induce so-called hydrophobic effects on the nature of water in the vicinity of the nonpolar alkyl group, which is manifested by a large enthalpy gain and an even larger entropy loss.[1−6] Since alcohol/water mixtures are recognized as the simplest yet typical prototype of biomolecules and micelle-forming systems, they have been subjected to a number of experimental and theoretical studies.[1−32] According to recent results,[22−24,27,33−49] the time scales of the cooperative relaxation process of H-bond liquids not only for water but also alcohols and their mixtures are generally governed by the probability that molecules in the systems find a new H-bond partner, so that the density of hydrophilic (i.e. H-bond donor and acceptor) sites is one of the dominating factors. Especially Kaatze and co-workers[24−27,39−42,50,51] made considerable efforts to combine the results of dielectric relaxation experiments with the concepts obtained from computer simulations by systematically comparing the relaxation times of various H-bonding liquids and binary systems plotted against the concentration of H-bond donor or acceptor sites. The technique of dielectric relaxation spectroscopy (DRS)[17−27,29−43,50−70] is especially suited for an investigation of the H-bond rearrangement dynamics, owing to its inherent ability to monitor the cooperative motion of a molecular ensemble through the response of the total dipole moment of samples to a time-dependent electric field via the complex permittivity spectrum, $\epsilon^*(\nu) = \epsilon' - i\epsilon''$. In ref 33, the recent development of DRS in liquid-state studies was thoroughly recapitulated. While this method is being applied to more and more complicated systems (see ref 55 for examples), a consistent description of $\epsilon^*(\nu)$ for alcohol/water systems that can lay the basis for the better understanding of other H-bond systems is still lacking. This has given rise to incoherent interpretations and opposing views of the cooperative dynamics in these systems and to difficulties in connecting some DRS results to inference from other methods.[17−25,29−32] The main source of the problem appears to be a too simple assumption on the shape of the spectra and/or an excessive emphasis upon numerical aspects of the applied fitting functions without providing sufficient statistical information, neglecting the necessary conformity between the relaxation behavior of the pure solvents. Incomplete understanding of the relaxation behavior of the pure components, an insufficient frequency coverage, and accuracy of the data may have been problematic in earlier works.

Recently, Bowron, Finney, and Soper performed the neutron diffraction (ND) studies on *tert*-butyl alcohol (TBA)/water mixtures[8,9] in the water-rich region and pure TBA using the

* To whom correspondence should be addressed. E-mail: sato@polymer.phys.waseda.ac.jp.

10.1021/jp035255o CCC: $27.50
Published on Web 05/13/2004

EPSR modeling procedure for data analysis.[10] Bowron et al. extended these investigations to a concentrated *tert*-butyl alcohol(TBA)/water mixture using the same method.[11] As the sequels, Dixit et al. performed ND studies on dilute[12] and a concentrated[13] aqueous methanol. According to the obtained water oxygen−oxygen radial distribution function (RDF), the water structure in the vicinity of a hydrophobic solute is not perturbed.[8,9,12,13] These results may challenge the generally accepted traditional concept of a structural enhancement of the hydrogen bond network of water by hydrophobic solutes, the so-called hydrophobic hydration, originating from Franks and Evans.[1]

To be able to make a contribution to this essential subject from the viewpoint of cooperative and molecular dynamics, it is urgent to establish a reliable model for the dynamics of alcohol/water mixtures. The goal of this study is to work out a numerically well- based but at the same time physically realistic relaxation model for ethanol/water mixtures that can consistently explain the concentration dependence of the $\epsilon^*(\nu)$ spectra measured up to 89 GHz over the entire mixing range and simultaneously conforms to the well-established models for the relaxation behavior of the pure solvents.

2. Experimental Section

The Complex Permittivity Measurements. The solutions were prepared by weight from A-grade reagent ethanol (Wako and Merck) and Millipore water. The ethanol sample was used as received. We have determined the $\epsilon^*(\nu)$ spectra of ethanol/water mixtures at the molar fractions of ethanol, $X_{EA} = 0.04$, 0.08, 0.11, 0.18, 0.3, 0.5, 0.7, 0.9, and 1.0 at 25 °C in the frequency range $0.1 \leq \nu/\mathrm{GHz} \leq 89$. Time Domain Reflectometry (TDR)[17−23,53,62] was employed in the frequency range of $0.1 \leq \nu/\mathrm{GHz} \leq 25$, and the TDR data were combined with those obtained with the three waveguide interferometers in the Ku, A, and E band[53] covering $13 \leq \nu/\mathrm{GHz} \leq 89$. For ethanol ($X_{EA} = 1.0$), the TDR data in $0.1 \leq \nu/\mathrm{GHz} \leq 25$ newly obtained in this study were combined with the interferometry data of Barthel et al.[33,51] in $0.9 \leq \nu/\mathrm{GHz} \leq 89$. Temperature control was made with an accuracy of ±0.02 °C for TDR measurements and ±0.03 °C for interferometry. We confirmed that TDR data completely match with Ku-band ($13 \leq \nu/\mathrm{GHz} \leq 17.5$) interferometer data in the overlapping range for all the investigated solutions and are smoothly connected to A-band ($27 \leq \nu/\mathrm{GHz} \leq 39$) and E-band ($60 \leq \nu/\mathrm{GHz} \leq 89$) data. The basic part of the experimental setup for TDR and the waveguide interferometers and of the measurement procedures and the accuracy of the data have been discussed elsewhere.[17−19,53,54,62]

The New TDR Procedures. In this study, we have applied the updated advanced techniques to TDR measurements. We employed the *time-window divided modified direct* method (the TDMD method), in which wave forms of the reflected pulse from standard and unknown samples were recorded by using multiple time windows with a short time/div of a digitizing oscilloscope (HP54120B) with optimized different delay times for the individual divided time windows, and these planes were combined into one wave form to increase a time resolution of the time domain measurements and simultaneously to maintain the total length of time windows for the sufficient low-frequency limit. We carefully took static permittivity (ϵ) dependence of the electric cell length of the conductor and flat-end capacitor cells,[53,62] *d*, into account, referring to *d* estimated from iterative measurements of various standard samples as a function of ϵ, which we call the $d(\epsilon)$-calibration procedure. In addition, we employed the independent *d* Fourier transform for the calculation of the complex dielectric permittivity, $\epsilon^*(\nu)$, for which, different from the conventional approach, the independent electric cell lengths for standard and unknown samples were used for the Fourier transform of the differential waveform between the reflected pulses from standard and unknown samples.

Note that conventional assumptions that the electric cell length, *d*, is basically equal to a mechanical pin length of a conductor cell, and $d = 0.01$ mm is a sufficient approximation for a flat-end capacitor cell with a zero mechanical length need urgent correction. Especially the latter may have caused deformation of a water-rich spectrum shape especially marked at high ν in earlier TDR studies. Although it is said that *d* can be estimated from the high-frequency part of a standard spectrum, it is not trivial to estimate *d* accurately for the conductor cells only from standard measurements. However, even the empirical correction of $d = d_{mech} + \Delta d$, where Δd is an arbitrarily added correction term of ∼0.3 mm considering a leakage of an electric field, is not always sufficient. We determined the cell constant *gd* from the extrapolated static permittivity of standard samples, where *g* is the normalization coefficient of the characteristic impedance between the feeding line, $Z_0 = 50\ \Omega$, and the sample section, *Z*. We calculated *g* using the following equations according to Buchner's suggestion,[53]

$$Z = \frac{1}{2\pi}\sqrt{\frac{\mu_0}{\epsilon_0}}\ln\left(\frac{l_2}{l_1}\right) \tag{1}$$

and

$$g = Z/Z_0 \tag{2}$$

where l_1 and l_2 are the diameter of the inner and outer conductor of the cell, and ϵ_0 and μ_0 are permittivity and permeability of the vacuum, respectively. From the experimentally obtained cell constant, *gd*, and the calculated *g*, the electric cell length, *d*, was estimated. We think that this is the best possible method so far. Actually only this method can provide a perfect match among spectra measured by a number of conductor cells with various d_{mech}, l_1, and l_2 values in the overlapping measurable frequency range.

As for the flat-end capacitor cell without an extended outer conductor, the method suitable for the conductor cells mentioned above needs modifications. Equations 1 and 2 are not perfectly valid due to complicated leakage effects of an electric field at the flat end of the cell. In this case, iterative measurements of the samples with a high loss peak frequency such as water, acetone, acetonitrile, and so on, whose high-frequency data (especially dielectric loss) are very sensitive to the value of *d*, are helpful for the estimation of *d*. The appropriate value for the flat-end cell with a zero mechanical length and a 2.2-mm diameter is $d \approx 0.29$ mm, being fairly different from the conventional $d = 0.01$ mm. The value of *g* is fixed for the $d(\epsilon)$-calibration procedure for all types of sample cells. We will report the details of the procedures elsewhere soon.

3. Data Analysis

Using a nonlinear least-squares fitting procedure based on the Gauss−Marquart algorithm we thoroughly tested various conceivable relaxation models,

$$\epsilon^*(\nu) = \epsilon_\infty + \sum_{j=1}^{n}\frac{\Delta\epsilon_j}{[1 + (i2\pi\nu\tau_j)^{\beta_j}]^{\alpha_j}} \tag{3}$$

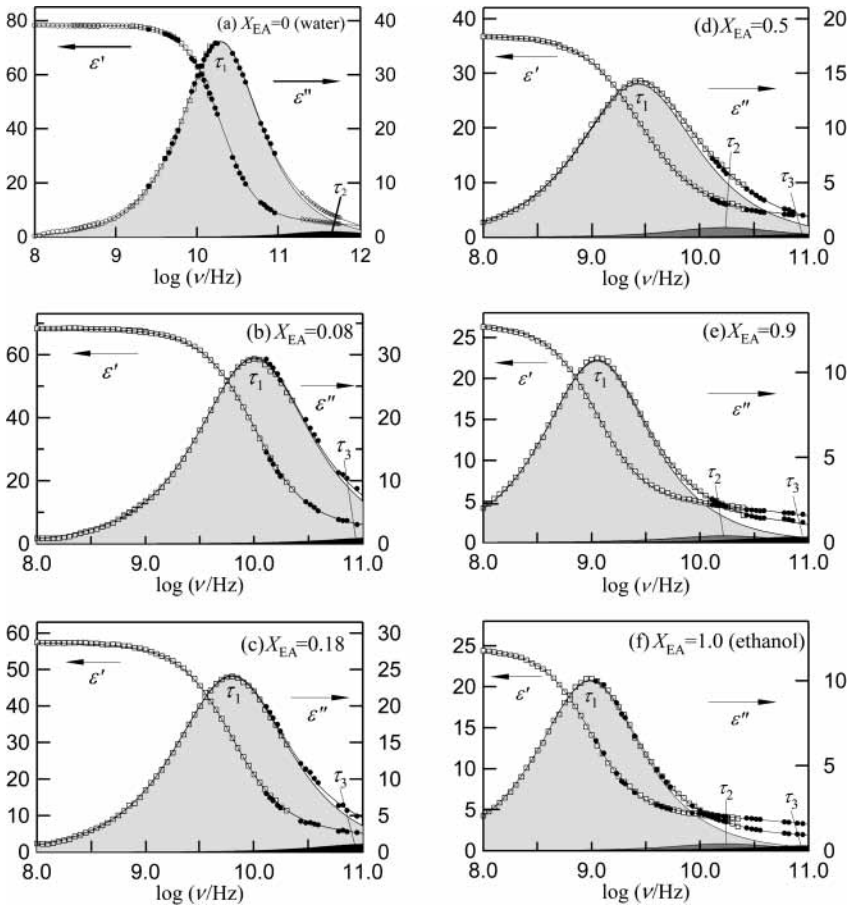

Figure 1. Dielectric dispersion, $\epsilon'(\nu)$, and loss, $\epsilon''(\nu)$, spectra of ethanol/water mixtures at 25 °C [$X_{EA} = 0$ (a), 0.08 (b), 0.18 (c), 0.5 (d), 0.9 (e), and 1.0 (f)] determined with TDR (□) and waveguide interferometry (●). (a) $X_{EA} = 0$, the spectrum of water in $0.1 \le \nu$/GHz ≤ 561, was obtained in ref 37; TDR data (○) and waveguide interferometry data (●), including the interpolated far-infrared data (◇) in $195 \le \nu$/GHz ≤ 561 of Rønne et al.[38] and TDR data (□) of Sato et al.[62] For (f) X_{EA}=1.0 (ethanol), newly obtained TDR data (□) in $0.1 \le \nu$/GHz ≤ 25 were combined with the interferometry data (●) of Barthel et al.[33] in $0.95 \le \nu$/GHz ≤ 89.

based on a superposition of n Havriliak−Negami (HN) equations, or its variants, Davidson−Cole (DC), Cole−Cole (CC), or Debye (D) equations,[71] to fit the experimental complex permittivity spectra. In the models the jth dispersion step (j = 1, 2, ..., n) is defined by its relaxation time, τ_j ($\tau_j > \tau_{j+1}$), and relaxation amplitude, $\Delta\epsilon_j$, where n is the number of separable dispersion steps, ϵ_∞ is the infinite frequency permittivity, and α_j and β_j are shape parameters representing an asymmetric and a symmetric shape of a spectrum, respectively. The (extrapolated) static permittivity, ϵ_S, can be defined as

$$\epsilon_S = \lim_{\nu \to 0} \epsilon'(\nu) = \epsilon_\infty + \sum_{j=1}^{n} \Delta\epsilon_j \qquad (4)$$

We fitted eq 3 simultaneously to the dispersion, ϵ', and the loss, ϵ'', of the measured $\epsilon^*(\nu)$ spectrum to obtain the absolute minimum value of the reduced error function, χ^2,

$$\chi^2 = \frac{1}{2N - m - 1}\left[\omega'(\nu_i)\sum_{i=1}^{N}\delta\epsilon'(\nu_i)^2 + \omega''(\nu_i)\sum_{i=1}^{N}\delta\epsilon''(\nu_i)^2\right] \qquad (5)$$

where $\delta\epsilon'(\nu_i)$ and $\delta\epsilon''(\nu_i)$ are the residuals for the dispersion, ϵ', and the loss, ϵ'', N is the number of data triples (ν_i, ϵ', ϵ''), m is the number of the adjustable parameters, and $\omega(\nu_i)$ is the weight function.

4. Results and Discussion

In Figure 1, we display the $\epsilon^*(\nu)$ spectra of the ethanol/water mixtures at 25 °C at X_{EA}= 0 (a), 0.08 (b), 0.18 (c), 0.5 (d), 0.9 (e), and 1.0 (f), which visualize the quality of the data and the consistently excellent fit. For the endpoints, the spectrum of pure water ($X_{EA} = 0$) in $0.1 \le \nu$/GHz ≤ 561[22,37] including the interpolated far-infrared data in $195 \le \nu$/GHz ≤ 561 of Rønne et al.[38] were adopted, and for neat ethanol ($X_{EA} = 1.0$), the TDR data in $0.1 \le \nu$/GHz ≤ 25 obtained in this study were combined with the interferometer data of Barthel et al.[34,52] in $0.95 \le \nu$/GHz ≤ 89.

The relaxation time of water for the main dispersion step, $\tau_1 \approx 8$ ps at room temperature, reflects the time scale of the cooperative rearrangement of the H-bond network.[22,23,27,34,36−38,43−47,50−52,60] Barthel et al.,[34] analyzing their interferometer data together with far-infrared results of Hasted et al.,[70] were able to separate an additional high-frequency process with a relaxation time $\tau_2 < 1$ ps at room temperature. Assuming that water molecules with four, three, and two H-bonds are trapped into the H-bond network to be released only when all but (maximally) one hydrogen bonds are broken, the relaxation time τ_1 was interpreted as the dwelling time of a H_2O molecule until it is released and can rapidly rotate with τ_2 into a different favorable configuration.[22,23,36] Note that according to this study, τ_1 and τ_2 are characteristic times for two subsequent steps in a single chain of events leading to the reorientation of an individual water molecule, but are *not*

indicators of two coexisting substates of water in the liquid. This interpretation may contrast with that of Okada et al.,[43] who made dielectric relaxation measurements on water and heavy water in $0.04 \leq \nu/\mathrm{GHz} \leq 40$ in the whole fluid by the use of the specially constructed apparatus based on a network analyzer. They suggested a two-state model, in which the liquid phase consists of a mixture of high-temperature liquid like a gaseous state and a strongly connected low-temperature liquid. Under the assumption that bound water molecules and free water molecule have distinct relaxation times, they introduced a model in which the observable τ_1 for water is given by the average $\tau_1 = \tau_{\mathrm{col}} + f_{\mathrm{B}}\tau_{\mathrm{lib}} \exp(H_{\mathrm{HB}}/k_{\mathrm{B}}T)$, where τ_{col} is a collision time, f_{B} the fraction of bound water molecules, and τ_{lib} the inverse of the mean librational frequency of bound water molecules.

Sufficient frequency coverage and accuracy especially for the high-frequency tail of spectra provide three relaxation processes for monohydric alcohols around room temperature. Since the pioneer work of Garg and Smyth in the 60's,[56] their assignment to the microscopic relaxation mechanisms has been discussed frequently.[22−24,33,34,52,56,61] This is in many cases corroborated by the dielectric relaxation behavior of supercooled monohydric alcohols, investigated by Brand,[64] Fischer,[65,66] Hansen,[66] Vij,[67−69] Johari,[68,69] and their co-workers, where three processes can be observed even when the temperature is close to the glass-transition temperature. Brand et al.[64] studied pure ethanol in the frequency range $3\mu < \nu/\mathrm{Hz} < 500$ M at temperatures $40 < T/\mathrm{K} < 230$, in which the second β process was identified as the excess wing from the main dispersion. If the relaxation times of the slowest α, the intermediate β, and the fastest γ processes of ethanol obtained in the supercooled temperature range are extrapolated to a high-temperature range, they are smoothly connected to the cooperative ($j = 1$), intermediate monomer ($j = 2$), and fast OH flipping ($j = 3$) processes in the three-Debye model at room temperature,[34,52] respectively.

The low-frequency main dispersion step ($j = 1$) with τ_1 ranging from 51 ps for methanol to 350 ps for 2-propanol at room temperature reflects the cooperative motion of H-bonded alcohol molecules,[33,36,51] which is attributed to the "interaction dynamics" between different hydrogen-bonded chains. In light of the accumulated experimental information,[23,33,−35,40,42,52] the time scale for τ_1 is governed by the strength of the H-bond as well as by the availability of alternative H-bond sites able to react with the just-released H-bond acceptor or/and donor. The comparison of pure 1-propanol and 2-propanol[23,34,37,52] and their mixtures with 1-phenyl-1-propanol and 1-phenyl-2-propanol[68,69] indicates that steric hindrance also plays an important role for the cooperative mode ($j = 1$).

Although the mechanism of the intermediate process ($j = 2$) with $\tau_2 \approx 10-20$ ps is still open for discussion, it has been assigned to the (not necessarily diffusive) motion of a singly H-bonded end-standing alcohol monomers in the chain structure. Without considering the existence of the $j = 2$ mode, the alcohol spectra can never be reproduced within the framework of a superposition of the conventional relaxation functions and/or distribution of relaxation time in a one-step relaxation model. We found in the present study that a single-Debye model can reproduce the ethanol spectrum only up to 4 GHz, above which the variance of the fit monitored at each ν steeply increases and the residual defined as $\delta\epsilon(\nu) = \epsilon(\nu)_{\mathrm{data}} - \epsilon(\nu)_{\mathrm{fit}}$ becomes systematically negative for the real part (ϵ') and positive for the imaginary part (ϵ''). The fast process ($j = 3$) with $\tau_3 \approx 1-2$ ps was assigned to a flipping motion of free OH groups.[22,23,34,37,52] The amplitude of the intermediate process, $\Delta\epsilon_2$, of monohydric alcohols determined in the temperature range $248.15 \leq T/\mathrm{K} \leq 328.15$ exhibits a clear tendency to increase with decreasing temperature.[37] Kalinovskaya and Vij showed that this also holds for 5-methyl-2-hexanol in the supercooled liquid and glassy states in $110 \leq T/\mathrm{K} \leq 298$.[67] They concluded that the intermediate process originates in a rotation of the OR group in the H-bonded chains, not a rotation of free molecules. If the τ_2 process were essentially due to the rotational diffusion of alcohol monomers one would indeed expect an opposite temperature dependence of $\Delta\epsilon_2$. However, it is unlikely that the motion of these "free" ethanol molecules can be described as an isotropic rotational diffusion. Hints from MD simulations suggest that this mode is in part connected with the formation of transient bifurcated hydrogen bonds[22,23,72,73] and in analogy to the situation in water[36] it appears that this mode reflects the "relocking" of the "free" alcohol molecule into the hydrogen bond system, but with different orientation and in a different chain.

As a major finding from the optimum fitting procedure, we found that in the ethanol-rich region of $0.3 \leq X_{\mathrm{EA}} \leq 1.0$, similar to pure alcohols, a three-step relaxation model is required to describe consistently the $\epsilon^*(\nu)$ spectra of the investigated mixtures in $0.1 \leq \nu/\mathrm{GHz} \leq 89$. The superposition of the Cole−Cole equation for the low-frequency main dispersion step ($j = 1$) and two additional high-frequency Debye ($j = 2$ and 3) terms with $\tau_2 \approx 10$ ps and $\tau_3 \approx 1-2$ ps, hereafter the "3CC" model, turns out to be most appropriate,

$$\epsilon^*(\nu) = \epsilon_\infty + \frac{\Delta\epsilon_1}{1 + (i2\pi\nu\tau_1)^\beta} + \frac{\Delta\epsilon_2}{1 + i2\pi\nu\tau_2} + \frac{\Delta\epsilon_3}{1 + i2\pi\nu\tau_3} \quad (6)$$

In the water-rich region of $0 \leq X_{\mathrm{EA}} < 0.3$, $\Delta\epsilon_2 \rightarrow 0$ and τ_1 approaches τ_2 for vanishing ethanol concentration, so that the intermediate process ($j = 2$) is no longer separable. Here, the $\epsilon(\nu)^*$ spectra are best modeled by the superposition of the Cole−Cole equation for the main dispersion step ($j = 1$) and an additional Debye equation for the fast switching process ($j = 3$) with $\tau_3 \approx 1$ ps (the "2CC" model),

$$\epsilon^*(\nu) = \epsilon_\infty + \frac{\Delta\epsilon_1}{1 + (i2\pi\nu\tau_1)^\beta} + \frac{\Delta\epsilon_3}{1 + i2\pi\nu\tau_3} \quad (7)$$

(Although the number of distinguishable dispersion steps is 2 in this region, we continue to use the notation of $j = 1$ and 3 to indicate the assignment to the main process and the fast switching process, respectively.) The results, summarized in Table 1, are consistent with our recent results of 2-propanol/water mixtures.[22,23] Table 2 compares the results of the fitting procedure with various models. In Figure 2, we display the residuals of the fit, $\delta\epsilon^k(\nu) = \epsilon^k(\nu)_{\mathrm{data}} - \epsilon^k(\nu)_{\mathrm{fit}}$, for the ethanol/water mixtures at $X_{\mathrm{EA}} = 1.0$ (a), 0.9 (b), 0.7 (c), 0.3 (d), and $X_{\mathrm{EA}} = 0.18$ (e) for dispersion (ϵ') and loss (ϵ''). The models chosen here as the most appropriate for physical reasons have a solid statistical basis, whose validity is well-supported by [1] the consistently excellent fit for the entire mixing range as shown in Figure 1, [2] the minimum variance as listed and compared in Table 2, [3] flat and nearly zero residual for the entire frequency range as displayed in Figure 2, and [4] good conformity to the well-established relaxation behavior of pure solvents.

We display the relaxation times of ethanol/water mixtures, τ_j, for the individual processes ($j = 1$, 2, and 3) together with those for 2-propanol/water mixtures[22] as a function of alcohol molar fraction, X_{A}, in Figure 3, the relaxation time of the cooperative process, τ_1, for various alcohol/water mixtures[17−23]

TABLE 1: Dielectric Relaxation Parameters for Ethanol/Water Mixtures in the "2CC" and "3CC" Models at Various Concentrations at 25 °C

X_{EA}	ϵ_s	τ_1/ps	$\Delta\epsilon_1$	b_1	τ_2/ps	$\Delta\epsilon_2$	τ_3/ps	$\Delta\epsilon_3$	ϵ_∞[a]	$\chi^2 \times 10^5$
0.00	78.25	8.32	72.15	1.000			0.39	2.14	3.96	2.186
0.04	73.20	11.97	67.58	0.978			0.56	1.92	3.70 F	4.190
0.08	68.30	15.85	62.84	0.958			1.12	1.86	3.60 F	5.090
0.11	64.79	18.97	59.34	0.954			0.65	1.90	3.55 F	5.863
0.18	57.32	25.48	51.76	0.954			1.46	2.16	3.40 F	5.104
0.30	47.73	35.98	42.45	0.940	7.44	0.86	1.25	1.49	3.14	2.642
0.50	36.94	59.57	31.07	0.934	9.50	1.79	1.08	1.21	2.87	3.091
0.70	30.81	94.41	25.39	0.956	8.91	1.44	1.39	1.28	2.70	3.035
0.90	26.50	142.2	21.73	0.988	9.57	0.77	1.97	1.32	2.68	3.652
1.00	24.47	164.9	19.94	1.000	10.4	0.74	1.69	1.19	2.60	3.243

[a] F indicates "fixed" for the fitting procedure.

TABLE 2: The Summary of the Results of the Fitting Procedure with Various Models: Dielectric Relaxation Parameters in Eq 3 for the Ethanol/Water Mixtures at Various Concentrations at 25 °C

model	τ_1/ps	$\Delta\epsilon_1$	α_1	β_1	τ_2/ps	$\Delta\epsilon_2$	τ_3/ps	$\Delta\epsilon_3$	ϵ_∞[a]	$\chi^2 \times 10^5$
[1] $X_{EA} = 0.08$										
(a) 1CC	15.64	63.57	1.000	0.952					4.82	7.079
(b) 1DC	19.44	65.21	0.812	1.000					2.69	5.436
(c) 1DC	19.44	65.21	0.812	1.000					2.69	5.436
(d) 2D	17.80	55.33	1.000	1.000			4.46	8.45	4.11	8.874
(e) 2CC	15.85	62.84	1.000	0.958			1.12	1.86	3.60 F	5.090
[2] $X_{EA} = 0.18$										
(a) 1CC	24.94	52.73	1.000	0.942					4.75	7.422
(b) 1DC	31.41	53.58	0.806	1.000					3.33	7.477
(c) 1DC	31.41	53.58	0.806	1.000					3.33	7.477
(d) 2D	28.62	45.29	1.000	1.000	7.10	7.09			4.52	13.06
(e) 2CC	25.48	51.76	1.000	0.939			1.46	2.16	3.40 F	5.103
[3] $X_{EA} = 0.30$										
(a) 1DC	46.43	44.50	0.767	1.000					2.72	9.790
(b) 1HN	38.79	44.20	0.907	0.946					3.50	3.002
(c) 2D	41.79	35.83	1.000	1.000	10.4	7.32			4.06	19.74
(d) 3D	44.21	32.63	1.000	1.000	15.2	9.73	1.30	1.93	3.15	15.57
(e) 3CC	35.98	42.45	1.000	0.940	7.44	0.86	1.25	1.49	3.14	2.642
[4] $X_{EA} = 0.70$										
(a) 1DC	121.3	27.37	0.744	1.000					3.20	5.550
(b) 1HN	118.6	27.39	0.760	0.991					3.24	5.245
(c) 2DC	117.3	27.00	0.773	1.000			1.23	0.93	2.59	3.547
(d) 2HN	105.0	26.74	0.857	0.968			2.31	1.11	2.86	1.584
(e) 2D	97.90	23.81	1.000	1.000	10.9	3.00			3.61	19.99
(f) 3D	110.0	20.43	1.000	1.000	37.4	5.24	3.44	3.06	3.06	6.405
(g) 3CC	94.41	25.39	1.000	0.956	8.91	1.44	1.39	1.28	2.70	3.035

[a] F indicates "fixed" for the fitting procedure.

against the molar concentration of H-bond acceptor sites, C_{HA}, in Figure 4, and the relaxation amplitudes, $\Delta\epsilon_j$ (j = 1, 2, and 3), and ϵ_∞ for ethanol/water and 2-propanol/water mixtures plotted against the volume fraction of alcohol, X_{VA}, in Figure 5.

In earlier studies with data restricted to $\nu_{max} \leq 20$ GHz, models based on a single Davidson−Cole equation (1DC) or in some case a single Havriliak−Negami equation (1HN) were preferably used to represent the asymmetric shape of alcohol/water spectra in the alcohol-rich region.[29−31] These one-step relaxation models may have been a convenient and plausible first approximation for the limited accuracy and frequency range. However, conformity to the relaxation behavior of pure solvents[34,52] was not seriously considered and no statistical information about the validity of the fit was provided. In fact, the deconvolution of the dielectric spectrum is not an easy task. We point out that it has to be done objectively but at the same time it is highly important to get not only the small variance with fewer parameters but also a complete set of relaxation parameters with realistic values and without a breaking point. Additionally, we note that to check the flat residual of the fit for the entire frequency range is quite important as a measure of validity of models. We monitored simultaneously the variance and the residual of the fit at each frequency. If the single-Debye model is used for pure ethanol ($X_{EA} = 1.0$), this can reproduce the spectrum only up to ~4 GHz, but causes a large deviation at higher frequencies, giving a steep increase of the variance with increasing ν. The ethanol spectrum is asymmetric and broader on the higher frequency side. However, when the 1DC and 1HN modesl are used for the asymmetric shape, not only does large deviation from the data points become especially marked at ν > 10 GHz but also a strongly oscillating residual over the entire frequency range is produced as shown in Figure 2a, which clearly refuses the 1DC and 1HN fit for pure alcohol. These findings prove that the deviation from the single-Debye behavior above ~4 GHz cannot be interpreted as a distribution of the relaxation time but as the excess wing caused by an additional relaxation process. Only the triple-Debye (3D) model[22,23,33,34,37,52,63] can resolve these problems for the spectra obtained up to 89 GHz.

Next if we apply the 1DC and 1HN models to the ethanol-rich mixtures such as $X_{EA} = 0.9$, 0.7, and 0.5; the situations, a large variance and an oscillating residual, are completely the same as that for neat ethanol, as Figure 2 demonstrates. This indicates the main characteristics of the neat alcohol spectrum still remain for the alcohol-rich spectra and a similar relaxation mechanism should be operative. The pattern of the oscillation

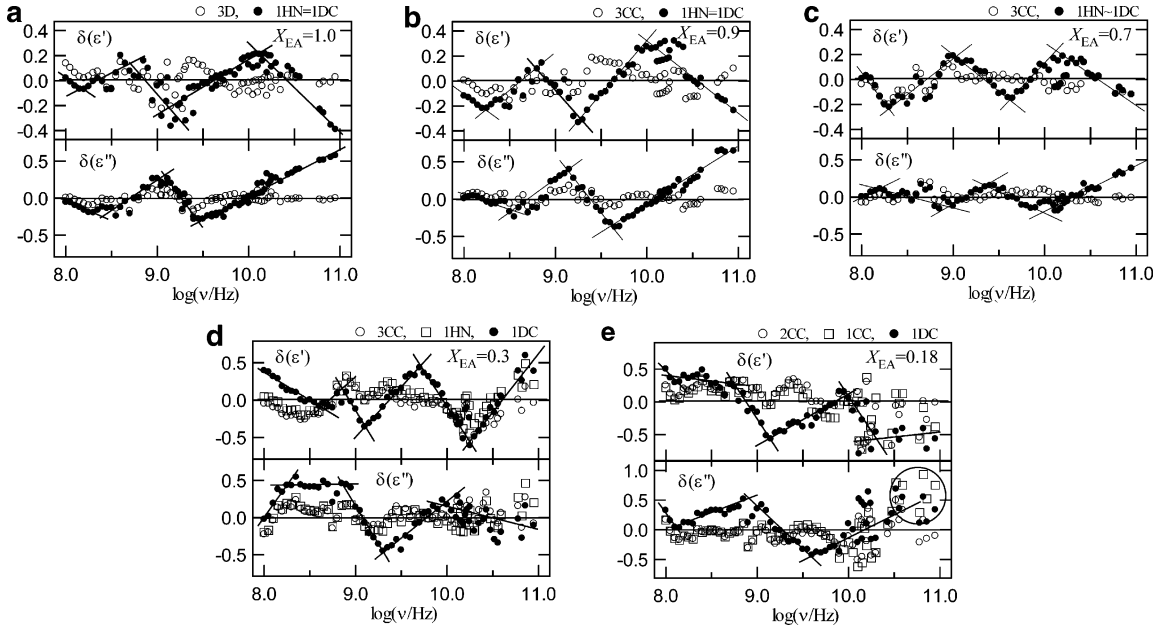

Figure 2. The residuals of the fit, $\delta\epsilon^k(\nu) = \epsilon^k(\nu)_{data} - \epsilon^k(\nu)_{fit}$, for ethanol/water mixtures at $X_{EA} = 1.0$ (a), 0.9 (b), 0.7 (c), 0.3 (d), and $X_{EA} = 0.18$ (e), where ϵ^k represents a dispersion (ϵ') and a loss (ϵ''), and the subscripts "data" and "fit" denote the experimental data and the fit value, respectively.

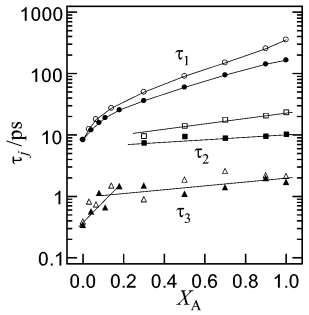

Figure 3. The relaxation times, τ_j ($j = 1$, 2, and 3), for ethanol/water (closed symbols) and 2-propanol/water mixtures[22] (open symbols) at 25 °C plotted against molar fraction of alcohol, X_A.

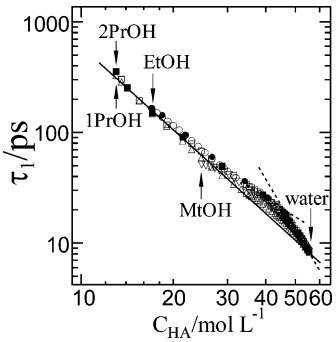

Figure 4. The relaxation times of the cooperative relaxation process, τ_1, for various alcohol/water mixtures at 25 °C: ethanol/water obtained in this study (●) and in ref 17 (○), methanol/water[18] (▽), 1-propanol/water[19] (△), and 2-propanol/water[22,23] (□ and ■), plotted against molar concentration of the hydrogen bond acceptor site in the mixtures, C_{HA}.

shows a change with increasing water content in $X_{EA} \geq 0.3$. We found that among the various models tested, only the 3CC model in the alcohol-rich region and the 2CC model in the water-rich region (in $X < 0.3$, the intermediate process becomes inseparable ($\Delta\epsilon_2 \rightarrow 0$), but it is natural to think that this is due to low alcohol content) satisfy the required conditions, giving excellent results of small variances, flat residuals close to zero in the entire measurable frequency range, and a complete set of the relaxation parameters which can consistently explain the

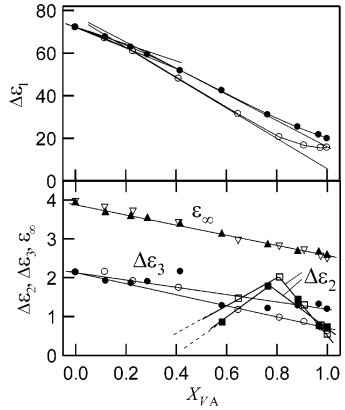

Figure 5. The concentration dependence of the relaxation amplitudes, $\Delta\epsilon_j$ ($j = 1$, 2, and 3), and the instantaneous permittivity, ϵ_∞, for ethanol/water (closed symbols) and 2-propanol/water mixtures[22] (open symbols) at 25 °C determined from the data in $0.1 \leq \nu/\text{GHz} \leq 89$ plotted against volume fraction of alcohol, X_{VA}.

concentration dependence. As examples [4] in Table 2 show, the variance of 1DC and 1HN fits to our $\epsilon^*(\nu)$ rapidly increases if the maximum frequency of the data used in the fit exceeds ~10 GHz and 1HN converges nearly to 1DC, $\alpha_1 \rightarrow 1$, for $X_{EA} = 0.9$, 0.7, and 0.5. These models can never reproduce the entire spectrum when ν_{max} reaches 89 GHz and exhibit systematic deviations. Inclusion of an additional high-frequency Debye term to the 1DC or 1HN models (the 2DC and 2HN models in Table 2) gives rather passable results in terms of the variance and the high-frequency relaxation time is rather similar to but longer than τ_3 of the 3CC model. However, especially for high ethanol contents, such as $X_{EA} = 0.9$ and 0.7, the absence of the alcohol monomer process, $\tau_2 \approx 10$ ps, in these models is in variance with the well-established triple-Debye (3D) relaxation behavior of pure alcohols.[22,23,33,34,37,52,63]

In the water-rich region of $0 < X_{EA} \leq 0.18$, the shape of the spectra gradually deviates form the Debye type with increasing X_{EA}. To obtain a small variance with the 1DC model for the spectra up to ~20 GHz, unusually small values of the instantaneous permittivity, ϵ_∞, are required. In view of $\Delta\epsilon_3 = 2.15$ and $\epsilon_\infty = 3.95$ for pure water,[22,37] $\epsilon_\infty < 3$ for the water-

rich mixtures without the high-frequency process is apparently too small. The combination of the 1DC model and quite small ϵ_∞ does not necessarily mean that the spectra are asymmetric but may indicate a nearly symmetric shape. The 1CC model yields reasonable values of $\epsilon_\infty \approx 5$ for the same concentration range, which are compatible with $\epsilon_\infty \approx 5.7$ determined with the 1D model for the water spectrum to $\nu_{max} \approx 25$ GHz and also with $\Delta\epsilon_3 + \epsilon_\infty$ obtained with the 2D model for $\nu_{max} = 561$ GHz.[22,37,38] In addition, the earlier assumption of the electric cell length $d = 0.01$ for a flat-end capacitor TDR cell may have led to artifactual asymmetric shapes of spectra especially for water-rich solutions.[29,30] Although the spectrum is not perfectly symmetric, a single Cole−Cole equation (1CC) is almost sufficient below ~40 GHz. However, marked systematic deviations appear for this model at $\nu > 60$ GHz as indicated by the circle in Figure 2e. A high-frequency Debye term must be added to the Cole−Cole equation for the main dispersion step, i.e., eq 7 is obtained. Due to the lack of far-infrared data, the ϵ_∞ determined for the water-rich mixtures are rather noisy, which influences the determination of τ_3 and $\Delta\epsilon_3$. To improve this situation for $0 < X_{EA} \leq 0.18$, we linearly interpolated ϵ_∞ as a function of ethanol volume fraction, X_{VEA}, between the values of water, $\epsilon_\infty(H_2O) = 3.95$,[22,36] and the ϵ_∞ obtained with eq 6 for the mixtures at $0.3 \leq X_{EA} \leq 1.0$ (Table 1). By presetting ϵ_∞ to the interpolated values in the fit, the 2CC model yields improved τ_3 and $\Delta\epsilon_3$ values with a smooth concentration dependence for $X_{EA} \leq 0.18$.

In view of the fact that τ_1 and $\Delta\epsilon_1$ exhibit a smooth transition from pure water ($\tau_1 = 8.27$ ps, $\Delta\epsilon_1 = 72.32$) to ethanol ($\tau_1 = 143$ ps, $\Delta\epsilon_1 = 19.98$) as shown in Figure 3 (τ_1) and Figure 5 ($\Delta\epsilon_1$), the main dispersion step ($j = 1$) of the mixtures is governed by a cooperative nature. The main dispersion ($j = 1$) can be assigned to the cooperative relaxation of the H-bond system composed of both water and alcohol, in which the motions of water and alcohol molecules cannot be distinguished. As discussed in refs 22 and 23, τ_1 can be interpreted as the lifetime of a locally stable configuration. Figure 3 contrasts the difference of $\tau_1(X_A)$ and $\tau_2(X_A)$ for different solute alcohols, which means that the activation quantities[17−21,23] for the τ_1-mode (the cooperative relaxation) clearly depend on solute alcohols, and τ_2 in the mixtures as well as neat alcohols reflects different alcohol molecular size. Taking up this different point of view, Figure 4 tries to explain the concentration dependence of τ_1 by generalization. The relaxation times, τ_1, for various alcohol/water systems[17−23] plotted against the molar concentration of H-bond acceptor sites, C_{HA}, are broadly on top of each other. This substantiates the view that the time scale of τ_1 is generally governed by the availability of alternative H-bond sites able to react with the released H-bond acceptor and/or donor. However, we found that the behavior of τ_1 is not completely linier against C_{HA}, and the deviation from the straight line becomes most marked at $C_{HA} \approx 45$ mol L^{-1}. The nonstraightforward behavior indicates that not only the mechanism dominated by the number density of the H-bond acceptor and donor sites but also the other effect caused by the specific interactions between water and alcohol is operative in the water-rich region. We point out that the finer difference of $\tau_1(C_{HA})$ among different alcohol/water systems seen in Figure 4 and the deviation of $\tau_1(C_{HA})$ from the ideal linear behavior in the water-rich region are quite essential, which becomes clear when the thermodynamic approach is applied.[17−22]

With increasing water content the relaxation time of the intermediate process ($j = 2$), τ_2, gradually decreases from $\tau_2 \approx 10$ ps of pure ethanol to ≈7 ps at $X_{EA} = 0.3$, the lowest alcohol concentration where this dispersion step could be resolved. The small amplitude, $\Delta\epsilon_2 < \sim 2$, remains compatible with that of pure ethanol. This suggests that the intermediate process ($j = 2$) for the mixtures can be assigned (at least mainly) to the motion of singly H-bonded end-standing ethanol molecules in the chains if the assignment is based on the accumulated information about dielectric behavior of pure alcohols.[22,23,33,34,37,52,64−69] The process possibly involves bifurcated hydrogen bonds as a transition state.[22,23,73] How water contributes to or affects this mode when a small amount of water is added to ethanol is of particular interest. The unexpected maximum of $\Delta\epsilon_2$ around an alcohol volume fraction of ~0.75 ($X_{EA} \approx 0.5$, see Figure 5) suggests an initial increase of the number of the end-standing ethanol molecules that can contribute to the $j = 2$ process. This may arise from the insertion of H_2O molecules into the zigzag H-bonded chain of alcohol molecules. The results of a RISM study on *tert*-butyl alcohol/water mixtures support this picture.[14] The decrease of $\Delta\epsilon_2$ at $X_{EA} < 0.5$, leading to its disappearance at $X_{EA} < 0.3$, is mainly due to low ethanol content and the speeding up of the cooperative dynamics, that is, τ_1 approaches τ_2. Thus, for the precision of our data the numerical separation of the $j = 2$ process becomes impossible at $X_{EA} < 0.3$ although a contribution of "free" ethanol molecules to the spectrum should continue to exist and is reflected in the concentration dependence of the Cole−Cole parameter, β_1, in this region.

As shown in Figures 3 and 5, the relaxation time, τ_3, and amplitude, $\Delta\epsilon_3$, of the fast process ($j = 3$) plotted respectively against the molar fraction (X_{EA}) and volume fraction (X_{VEA}) of ethanol show a smooth transition from ethanol to water, suggesting that for the mixtures this process can be attributed to the same moiety as for the fast processes of ethanol and water, that is the fast switching of free OH groups, either on unbound ethanol molecules or as singly H-bonded water molecules. In the free-energy landscape determining the molecular dynamics of alcohol/water mixtures both motions are almost equivalent and indistinguishable by DRS.

The orientational polarization of a sample ($\propto \epsilon_S - \epsilon_\infty$) is determined by the magnitude of the dipole moment of the constituting molecules, the number density of the dipolar species, and correlations of the average dipole orientations, expressed by the Kirkwood factor, g_K, for pure liquids. From the Kirkwood-Froehlich equation,[71] the effective dipolar moment of the mixtures may be defined as[23,24,39,41]

$$\mu_{eff}^2 = \frac{\epsilon_S - \epsilon_\infty}{\epsilon_S} \frac{2\epsilon_S + \epsilon_\infty}{(\epsilon_\infty + 2)^2} \frac{9kBT\epsilon_0}{cN_A} \tag{8}$$

where k_B is the Boltzmann constant, ϵ_0 the permittivity of vacuum, N_A the Avogadro number, and c the total concentration of dipoles. For the investigated mixtures this allows the definition of an effective correlation factor, g_{eff}, as

$$g_{eff} = c\mu_{eff}^2/(c_W\mu_W^2 + c_E\mu_E^2) \tag{9}$$

where c_W and c_E are respectively the molar concentration of water and ethanol, and $c = c_W + c_E$. For the dipole moments of water, $\mu_W = 1.84$D, and of ethanol, $\mu_E = 1.68$D, were used. As has been pointed out,[24−26,39,41] this definition of a correlation factor is a simplification since it averages over the per se different water−water, water−ethanol, and ethanol−ethanol correlations. However, the determination of individual correlation factors from dielectric data requires a number of assumptions.[74] A problem in the calculation of g_{eff} is the choice of the

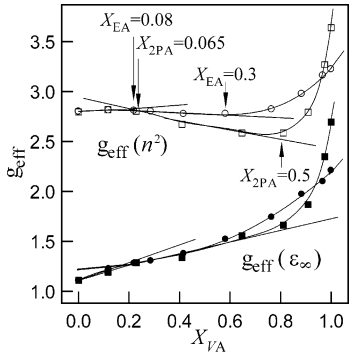

Figure 6. The concentration dependence of the effective orientational correlation factor, g_{eff}, for ethanol/water mixtures (● and ○) and 2-propanol/water mixtures (□ and ■) plotted against the volume fraction of alcohol, X_{VA}. g_{eff} was calculated with ϵ_∞ determined for the spectra in $0.1 \leq \nu/\mathrm{GHz} \leq 89$ (● and ■) and with the squared refractive index (n^2) for ϵ_∞ in eq 8 (○ and □) at 25 °C.

instantaneous permittivity.[71] Neither the result extrapolated from the DRS spectra with $\nu_{max} = 89$ GHz nor the square of the refractive index[75] at optical frequencies is the optimum choice because they apparently over- and underestimate ϵ_∞, respectively, which should incorporate all contributions but orientational polarization. In Figure 6, the concentration dependence of g_{eff} for ethanol/water and 2-propanol/watert mixtures[22] plotted against the volume fraction of alcohol, X_{VA}, is displayed for both limiting cases. Although the magnitude and the slope of g_{eff} are different, a similar pattern appears for the concentration dependence. Therefore, we believe that for alcohol/water mixtures g_{eff} defined by eq 9 is nevertheless a reasonable measure for the dipole−dipole correlations.

Pure 2-propanol shows a larger value of g_{eff} than pure ethanol (at $X_{VA} = 1$). 2-Propanol exhibits the relatively larger orientational polarization, $\sum\Delta\epsilon_j$, than ethanol expected from the number density of dipole. Although upon an addition of water to alcohol $\Delta\epsilon_1$ increases due to an increase of the number density of dipolar species, we found as shown in Figure 5 that first it gradually increases with increasing water content in $1 \geq X_{VA} \geq \sim 0.75$, and then changes into a linear-like steep increase in $\sim 0.75 \geq X_{VA}$. Furthermore, an increasing scheme of $\Delta\epsilon_1$ at the alcohol-rich side is different for the different solute alcohols, the 2-propanol/water system showing a more gradual increase. Strongly linked with these phenomena, as Figure 6 shows, when water is added to neat alcohols, the steep decrease of g_{eff} with increasing water content in $X_{VA} > \sim 0.7$ appears, and this is more pronounced in 2-propanol/water mixtures than in ethanol/water mixtures. This means that the parallel arrangement of dipole vectors of the alcohol molecules resulting from the hydrogen bonding to chain structures is fairly disturbed by the presence of a small amount of water, and the perturbation effect of water is larger for the larger alcohol. As we have mentioned, in the corresponding concentration region, $\Delta\epsilon_2$, assigned to the contribution of end-standing alcohol molecules,[22−24] increases despite decreasing alcohol content, suggesting an increase of end-standing alcohol molecules as a result of production of short alcohol chains due to insertion of water molecules into a zigzag H-bonded chain structure. According to the thermodynamic study of Koga et al.,[4] in alcohol-rich solutions, the enthalpic and entropic water−water interactions, H^E_{WW} and S^E_{WW}, bear the relation $0 > TS^E_{WW} > H^E_{WW}$, indicating that the water−water interaction is respectively repulsive and attractive in terms of entropy and enthalpy, and the stronger enthalpic attraction than the entropic repulsion will lead to self-aggregation of water molecules. In fact, self-aggregation of water and tighter packing of nonpolar groups in a concentrated TBA/water system were observed in the ND study of Bowron et al. For various alcohol/water systems, as Sato et al. reported,[17−21,23] the excess partial molar activation enthalpy and entropy for water, ΔH^E_W and ΔS^E_W, at $X_A \sim 1$ become positive, originating in the increase of ΔH^E and ΔS^E with increasing water content at the alcohol-rich side. The water added to alcohol has a distinct effect of enlarging the activation enthalpy and entropy of the mixtures more than expected from an ideal mixing, which implies a kind of structural enhancement. Combining all these features, here we suggest that a water-induced hydrophobic interaction even in the alcohol-rich side takes place, which is possibly connected with and/or somewhat similar to the mechanism of an inverse micelle structure formation.

On the other hand, starting form the water-rich side, with increasing ethanol content, first two linear parts of g_{eff} (X_{EA}) are observed with a change of slope at $X_{EA} \approx 0.08$, a critical concentration also for the activation parameters of τ_1,[17] which is followed by a pronounced nonlinear increase of g_{eff} at $X_{EA} \geq 0.3$. In the water-rich region corresponding to X_A(molar fraction of alcohol) > ∼0.1, g_{eff} for ethanol/water and that for 2-propanol/water coincide well with each other, but with the rise of alcohol content, as the nature of alcohol becomes gradually dominant, g_{eff} values for the two systems show clear separation, the 2-propanol/water system always exhibiting smaller values except for $X_A > \sim 0.9$.

The above discussion shows that for ethanol/water mixtures the description of $\epsilon^*(\nu)$ with the 3CC model at high and the 2CC model at low alcohol content is self-consistent and physically valid. What remains here is a comparison with previously published investigations that generally used other relaxation models. Sudo et al. studied 22 kinds of alcohol/water mixtures including sevral monohydric alcohol/water mixtures, in which they used a single Kohlrausch−Williams−Watts (KWW) function to fit the spectra measured up to ∼30 GHz.[32] They observed systematic changes of the KWW distribution parameter, β_{KWW}, and attempted a physical interpretation of the concentration dependence of β_{KWW}. We think that for monohydric alcohol/water mixtures at least in the alcohol-rich region, their β_{KWW} involves contributions of the τ_2-mode. Petong et al.[24] used the double-Debye model (the 2D model) to describe the spectra of ethanol/water mixtures measured up to 40 GHz. Being consistent with our present results, they also found the τ_2-mode with $\tau_2 \approx 10$ ps for the mixtures. To explain $\Delta\epsilon_2 \approx 10$ at maximum in their model, they assigned the τ_2-process to singly H-bonded end-standing dipolar groups of both ethanol and water. We argue that singly H-bonded H_2O molecules contribute to the $j = 3$ process with $\tau_3 = 1-2$ ps in terms of the behavior of τ_3 and $\Delta\epsilon_3$.

5. Conclusions

In light of the results of this investigation, a description of the $\epsilon^*(\nu)$ spectra for the ethanol/water mixtures based on a single Davidson−Cole (1DC) or Havriliak−Negami (1HN) model, frequently used in earlier works, has turned out to be insufficient for modeling the dynamics of monohydric alcohol/water systems, as proved by thorough statistical approaches including simultaneous monitoring of the residual and the variance of the fit. The dielectric relaxation behavior of the mixtures can be essentially linked to the relaxation mechanism of the pure solvents in terms of the number of the separable dispersion steps, the magnitudes of the relaxation time and amplitude of each relaxation process, and the concentration dependence of these parameters. The main dispersion step ($j = 1$) is assigned to the

cooperative dynamics of the H-bond system. τ_1, varying from 8.3 ps for water to 165 ps for ethanol, largely controlled by the number density of H-bond acceptor and donor sites in the binary mixtures, can be interpreted as the lifetime of a locally stable configuration in the energy landscape of the liquid. This low-frequency relaxation is specific to the H-bond systems and cooperative in nature, in which the contributions of alcohol and water cannot be distinguished. The motion of ethanol molecules at the ephemeral ends of chains of H-bonded molecules can be monitored ($j = 2$) not only for pure ethanol but also for the ethanol-rich mixtures with $X_{EA} \geq 0.3$. The concentration dependence of $\Delta\epsilon_2$ suggests an insertion of water molecules into the zigzag H-bonded structure. This mode may be connected with the formation of transient bifurcated hydrogen bonds. The fast switching motion of free OH groups, including a contribution of a singly H-bonded water, can be resolved ($j = 3$) for the entire mixing range. This mode monitors the rapid trapping of the local ensembles in a new, temporarily stable configuration.

Acknowledgment. The authors gratefully acknowledge the help of Prof. W. Kunz in providing access to all the facilities of his laboratory and many helpful discussions. We also thank Prof. A. Chiba for the use of the TDR system. This work was partly supported by the grant-in-aid for scientific research (C) and the 21st century center of excellence (COE) program, Waseda University, "Physics of self-organization systems composed of multi-components" from the Japan Society for the Promotion of Science (JSPS). T.S. acknowledges the generous support of the JSPS Young Research Fellowship DC2 and PD for his earlier works.

References and Notes

(1) Franks, H. S.; Evans, M. S. *J. Chem. Phys.* **1945**, *13*, 507.
(2) Koga, Y. *Can. J. Chem.* **1987**, *66*, 1187.
(3) Koga, Y.; Wong, T. Y. H.; Siu, W. W. Y. *Thermochim. Acta* **1990**, *169*, 27.
(4) Koga, Y.; Siu, W. W. Y.; Wong, T. Y. H. *J. Phys. Chem.* **1990**, *94*, 7700.
(5) Tamura, K.; Hu, J. H.; Trandum, C.; Westh, P.; Haynes, C. A.; Koga, Y. *Phys. Chem. Chem. Phys.* **2000**, *2*, 355.
(6) Tanaka, S. H.; Yoshihara, H. I.; Ho, A. W.-C.; Lau, F. W.; Westh, P.; Koga, Y. *Can. J. Chem.* **1996**, *74*, 713.
(7) Koga, Y. *Kotai Butsuri* **1995**, *37*, 172.
(8) Bowron, D. T.; Finney, J. L.; Soper, A. K. *J. Phys. Chem. B* **1998**, *102*, 3553.
(9) Bowron, D. T.; Soper, A. K.; Finney, J. L. *J. Chem. Phys.* **2001**, *114*, 6203.
(10) Bowron, D. T.; Finney, J. L.; Soper, A. K. *Mol. Phys.* **1998**, *93*, 531.
(11) Bowron, D. T.; Moreno, S. D. *J. Chem. Phys.* **2002**, *117*, 3753.
(12) Dixit, S.; Soper, A. K.; Finney, J. L.; Crain, J. *Europhys. Lett.* **2002**, *59*, 377.
(13) Dixit, S.; Crain, J.; Poon, W. C. K.; Finney, J. L.; Soper, A. K. *Nature* **2002**, *416*, 829.
(14) Yoshida, K.; Yamaguchi, T.; Kovalenko, A.; Hirata, F. *J. Phys. Chem. B* **2002**, *106*, 5042.
(15) Skaf, M. S.; Ladanyi, B. M. *J. Chem. Phys.* **1995**, *102*, 6542.
(16) Skaf, M. S.; Ladanyi, B. M. *J. Phys. Chem.* **1996**, *100*, 18258.
(17) Sato, T.; Chiba, A.; Nozaki, R. *J. Chem. Phys.* **1999**, *110*, 2508.
(18) Sato, T.; Chiba, A.; Nozaki, R. *J. Chem. Phys.* **2000**, *112*, 2924.
(19) Sato, T.; Chiba, A.; Nozaki, R. *J. Chem. Phys.* **2000**, *113*, 9748.
(20) Sato, T.; Chiba, A.; Nozaki, R. *J. Mol. Liq.* **2002**, *96*−*97*, 325.
(21) Sato, T.; Chiba, A.; Nozaki, R. *J. Mol. Liq.* **2002**, *101*, 99.
(22) Sato, T.; Buchner, R. *J. Chem. Phys.* **2003**, *118*, 4606.
(23) Sato, T.; Buchner, R. *J. Chem. Phys.* **2003**, *119*, 10789.
(24) Petong, P.; Pottel, R.; Kaatze, U. *J. Phys. Chem. A* **2000**, *104*, 7420.
(25) Kaatze, U.; Schäfer, M.; Pottel, R. *Z. Phys. Chem. Neue Folge* **1989**, *165*, 103.
(26) Kaatze, U.; Schumacher, A.; Pottel, R. *Ber. Bunsen-Ges. Phys. Chem.* **1991**, *95*, 585.
(27) Kaatze, U.; Behrends, R.; Pottel, R. *J. Non-Cryst. Solids* **2002**, *305*, 19.
(28) Nakanishi, K. *Bull. Chem. Soc. Jpn.* **1960**, *33*, 793.
(29) Mashimo, S.; Miura, N. *J. Chem. Phys.* **1993**, *99*, 9874.
(30) Mashimo, S.; Umehara, T.; Redlin, H. *J. Chem. Phys.* **1991**, *95*, 6257.
(31) Bao, J.-Z.; Swicord, M. L.; Davis, C. C. *J. Chem. Phys.* **1996**, *104*, 4441.
(32) Sudo, S.; Shinyasiki, N.; Kitsuki, Y.; Yagihara, S. *J. Phys. Chem. A* **2002**, *106*, 458.
(33) Buchner, R.; Barthel, J. *Annu. Rep. Prog. Chem., Sect. C* **2001**, *97*, 349.
(34) Barthel, J.; Bachhuber, K.; Buchner, R.; Hetzenauer, H. *Chem. Phys. Lett.* **1990**, *165*, 369.
(35) Buchner, R.; Barthel, J. *J. Mol. Liq.* **1992**, *52*, 131.
(36) Buchner, R.; Barthel, J.; Stauber, J. *Chem. Phys. Lett.* **1999**, *306*, 57.
(37) (a) Pickl, H.; Buchner, R.; Barthel, J. Unpublished results. (b) Pickl, H. Ph.D. Thesis, Regensburg, 1997.
(38) Rønne, C.; Thrane, L.; Åstrand, P. O.; Wallqvist, A.; Mikkelsen, K. V.; Keiding, S. R. *J. Chem. Phys.* **1997**, *107*, 5319.
(39) Wang, F.; Pottel, R.; Kaatze, U. *J. Phys. Chem. B* **1997**, *101*, 922.
(40) Petong, P.; Pottel, R.; Kaatze, U. *J. Phys. Chem. A* **1999**, *103*, 6114.
(41) Fuchs, K.; Kaatze, U. *J. Phys. Chem. B* **2001**, *105*, 2036.
(42) Schwerdtfeger, S.; Köhler, F.; Pottel, R.; Kaatze, U. *J. Chem. Phys.* **2001**, *115*, 4186.
(43) Okada, K.; Yao, M.; Hiejima, Y.; Kouno, H.; Kajihara, Y. *J. Chem. Phys.* **1999**, *110*, 3026.
(44) Ohmine, I.; Tanaka, H.; Wolynes, P. G. *J. Chem. Phys.* **1988**, *89*, 5852.
(45) Tanaka, H.; Ohmine, I. *J. Chem. Phys.* **1987**, *87*, 6128.
(46) Ohmine, I.; Tanaka, H. *Chem. Rev.* **1993**, *93*, 2545.
(47) Ohmine, I. *J. Phys. Chem.* **1995**, *89*, 6767.
(48) Sciortino F.; Fornili, S. L. *J. Chem. Phys.* **1989**, *90*, 2786.
(49) Sciortino F.; Geiger, A.; Stanley, H. E. *J. Chem. Phys.* **1992**, *96*, 3857.
(50) Kaatze, U. *J. Chem. Eng. Data* **1989**, *34*, 371.
(51) Kaatze, U. *Chem. Phys. Lett.* **1993**, *203*, 1.
(52) Barthel, J.; Buchner, R. *Pure Appl. Chem.* **1991**, *63*, 1473.
(53) Buchner, R.; Barthel, J. *Ber. Bunsen-Ges. Phys. Chem.* **1997**, *101*, 1509.
(54) Barthel, J.; Bachhuber, K.; Buchner, R.; Hetzenauer, H.; Kleebauer, M. *Ber. Bunsen-Ges. Phys. Chem.* **1991**, *95*, 853.
(55) Baar, C.; Buchner, R.; Kunz, W. *J. Phys. Chem. B* **2001**, *105*, 2906.
(56) Garg, S. K.; Smyth, C. P. *J. Phys. Chem.* **1965**, *67*, 1294.
(57) Buchner, R.; Hefter, G.; May, P. M. *J. Phys. Chem. A* **1999**, *103*, 1.
(58) Buchner, R.; Capewell, S. G.; Hefter, G.; May, P. M. *J. Phys. Chem. B* **1999**, *103*, 1185.
(59) Buchner, R.; Hefter, G.; May, P. M.; Sipos, P. *J. Phys. Chem. B* **1999**, *103*, 11186.
(60) Agmon, N. *J. Phys. Chem.* **1996**, *100*, 1072.
(61) Buchner, R.; Yarwood, J. *Mikrochim. Acta* **1988**, *2*, 335.
(62) Sato, T.; Niwa, H.; Chiba, A.; Nozaki, R. *J. Chem. Phys.* **1998**, *108*, 4138.
(63) Garg, S. K.; Smyth, C. P. *J. Phys. Chem.* **1965**, *67*, 1294.
(64) Brand, R.; Lunkenheimer, U.; Schneider, R.; Loidl, A. *Phys. Rev. B* **2000**, *62*, 8878.
(65) Stickel, F.; Fischer, E. W.; Richert, R. *J. Chem. Phys.* **1994**, *104*, 2043.
(66) Hansen, C.; Stickel, F.; Berger, T.; Richert, R.; Fischer, E. W. *J. Chem. Phys.* **1997**, *107*, 1086.
(67) Kalinovskaya, O. E.; Vij, J. K. *J. Chem. Phys.* **2000**, *112*, 3262.
(68) Johari, G. P.; Kalinovskaya, O. E.; Vij, J. K. *J. Chem. Phys.* **2001**, *114*, 4634.
(69) Kalinovskaya, O. E.; Vij, J. K.; Johari, G. P. *J. Phys. Chem. A* **2001**, *105*, 5061.
(70) Hasted, J. B.; Husain, S. K.; Frescura, F. A. M.; Birch, J. R. *Infrared Phys.* **1987**, *27*, 11.
(71) (a) Böttcher, C. F. J. *Theory of Electric Polarization*, 2nd ed.; Elsevier: Amsterdam, The Netherlands, 1973; Vol. 1. (b) Böttcher, C. F. J.; Bordewijk, P. *Theory of Electric Polarization*, 2nd ed.; Elsevier: Amsterdam, The Netherlands, 1978; Vol. 2.
(72) Saiz, L.; Guàrdia, E.; Padró, J.-A. *J. Chem. Phys.* **2000**, *113*, 2814.
(73) Weingärtner, H.; Geiger, A. Private communication.
(74) Winkelmann, J.; Quitzsch, K. *Z. Phys. Chem.* **1976**, *257*, 678.
(75) Arce, A.; Blance, A.; Soto, A.; Souza, P.; Vidal, I. *Fluid Phase Equilib.* **1993**, *87*, 347.